



RESEARCH ARTICLE

10.1002/2015JD024698

Key Points:

- Regionally resolved impact of ENSO propagates into the stratosphere
- ENSO modulates the entry value of H₂O into the stratosphere
- ENSO has a regional influence on the Brewer-Dobson circulation

Correspondence to:

P. Konopka,
p.konopka@fz-juelich.de

Citation:

Konopka, P., F. Ploeger, M. Tao, and M. Riese (2016), Zonally resolved impact of ENSO on the stratospheric circulation and water vapor entry values, *J. Geophys. Res. Atmos.*, 121, 11,486–11,501, doi:10.1002/2015JD024698.

Received 5 JAN 2016

Accepted 11 SEP 2016

Accepted article online 16 SEP 2016

Published online 10 OCT 2016

Zonally resolved impact of ENSO on the stratospheric circulation and water vapor entry values

Paul Konopka¹, Felix Ploeger¹, Mengchu Tao¹, and Martin Riese¹¹Forschungszentrum Jülich (IEK-7: Stratosphere), Jülich, Germany

Abstract Based on simulations with the Chemical Lagrangian Model of the Stratosphere (CLaMS) for the period 1979–2013, with model transport driven by the ECMWF ERA-Interim reanalysis, we discuss the impact of the El Niño Southern Oscillation (ENSO) on the variability of the dynamics, water vapor, ozone, and mean age of air (AoA) in the tropical lower stratosphere during boreal winter. Our zonally resolved analysis at the 390 K potential temperature level reveals that not only (deseasonalized) ENSO-related temperature anomalies are confined to the tropical Pacific (180–300°E) but also anomalous wave propagation and breaking, as quantified in terms of the Eliassen-Palm (EP) flux divergence, with strongest local contribution during the La Niña phase. This anomaly is coherent with respective anomalies of water vapor (± 0.5 ppmv) and ozone (± 100 ppbv) derived from CLaMS being in excellent agreement with the Aura Microwave Limb Sounder observations. Thus, during El Niño a more zonally symmetric wave forcing drives a deep branch of the Brewer-Dobson (BD) circulation. During La Niña this forcing increases at lower levels (≈ 390 K) over the tropical Pacific, likely influencing the shallow branch of the BD circulation. In agreement with previous studies, wet (dry) and young (old) tape recorder anomalies propagate upward in the subsequent months following El Niño (La Niña). Using CLaMS, these anomalies are found to be around +0.3 (−0.2) ppmv and −4 (+4) months for water vapor and AoA, respectively. The AoA ENSO anomaly is more strongly affected by the residual circulation ($\approx 2/3$) than by eddy mixing ($\approx 1/3$).

1. Introduction

Water vapor in the tropical lower stratosphere is a powerful greenhouse gas and important driver of climate variability [Solomon *et al.*, 2010; Dessler *et al.*, 2013; Hegglin *et al.*, 2014]. Beyond the annual cycle (tape recorder), the interannual variability is mainly influenced by the quasi-biennial oscillation (QBO, mean period of 28 to 29 months) [Baldwin *et al.*, 2001; Dessler *et al.*, 2013], by the El Niño Southern Oscillation (ENSO) [Scaife *et al.*, 2003; Randel *et al.*, 2009], by major Sudden Stratospheric Warmings (mSSW) [Tao *et al.*, 2015], and to a weaker extent by the solar variability [Schieferdecker *et al.*, 2015]. Using model simulations, Scaife *et al.* [2003] found a significant moistening of the tropical lower stratosphere after warm ENSO events (El Niño) with signatures resembling the tape recorder signal [Geller *et al.*, 2002]. Trajectory-based studies driven by meteorological reanalysis have shown that at least strong El Niño situations (like 97/98) have a moistening impact (of a few tenths of a ppmv over a period of several months) and cold ENSO events (La Niña) have a smaller drying impact [Bonazzola and Haynes, 2004; Fueglistaler and Haynes, 2005].

Based on zonally averaged radiosonde and satellite observations, Randel *et al.* [2009] found that during El Niño the tropical lower stratosphere becomes colder and is associated with a negative ozone anomaly in this region. Contrarily, during La Niña a warmer lower stratosphere is accompanied by a positive ozone anomaly. Consistent with the ozone anomaly, Calvo *et al.* [2010] found that the Brewer-Dobson (BD) circulation strengthens during El Niño events whereas during La Niña an opposite signal of weakening BD circulation could be diagnosed. Using the Whole Atmosphere Community Climate Model (WACCM), they also identified ENSO-induced anomalies in the location and in the intensity of the subtropical jets as the main reason for different propagation and dissipation patterns of parameterized gravity waves and, consequently, for stronger (weaker) BD circulation during El Niño (La Niña) winter.

In this paper, we follow the spirit of these investigations. However, we extend the zonally averaged view to a longitudinally resolved analysis of temperature, Eliassen-Palm (EP) flux, water vapor, ozone, and mean age of air (AoA) anomalies. A regionally resolved view on the processes coupling the ENSO variability with the stratosphere has been adopted in several previous studies: Krüger *et al.* [2008] have shown the respective

©2016. The Authors.

This is an open access article under the terms of the Creative Commons Attribution-NonCommercial-NoDerivs License, which permits use and distribution in any medium, provided the original work is properly cited, the use is non-commercial and no modifications or adaptations are made.

variability of the location of the (Lagrangian) cold point, and *Liess and Geller* [2012] discussed the nonlinear impact of the QBO on the ENSO-related variability of tropical deep convection. As recently pointed by *Garfinkel et al.* [2013], differences in the impact of El Niño on the stratospheric water vapor may also depend on its maximum relative to the winter season (early or late winter/spring) and/or on its location (Central or Eastern Pacific). By using climate model simulations extending over 50 years, they found higher stratospheric entry values of ≈ 0.5 ppmv (≈ 0.3 ppmv) if El Niño peaks in late winter/spring (over Eastern Pacific).

In contrast to the QBO or solar variability which are global, downward propagating, and almost zonally symmetric perturbations of the atmospheric flow, the source of ENSO can be clearly localized in the tropical Pacific region. Thus, the propagation of the ENSO signal into the lower stratosphere has a significant longitudinal dependence with the strongest La Niña and El Niño signals in the Western and the Eastern Pacific, respectively. *Calvo-Fernandez et al.* [2004] found a very localized, ENSO-related source of temperature variability in the zonally resolved temperature Microwave Sounding Unit (MSU) observations, mainly in the upper tropical troposphere.

The key driver of the BD circulation in the stratosphere is the momentum transfer by planetary Rossby waves. Although Rossby waves are transient events per se, which are equally likely everywhere along the mostly zonally directed atmospheric jets, their spatial and temporal occurrence shows some systematic patterns. These patterns can be linked to the orography or seasonality and, as we will show later, are also related to a strongly localized ENSO variability. Therefore, we use a 3-D description as first proposed by *Plumb* [1985] and extend the common EP flux diagnostics of the zonally averaged eddy fluctuations [*Andrews et al.*, 1987].

We also quantify the impact of the ENSO anomaly on the transport of water vapor, ozone, and AoA from the Tropical Tropopause Layer (TTL) into the ascending branch of the BD circulation. To get statistically robust results we use 35 years of the ERA-Interim reanalysis [*Dee et al.*, 2011] covering the period 1979–2013 as well as the respective output of the Chemical Lagrangian Model of the Stratosphere (CLaMS) [*McKenna et al.*, 2002; *Konopka et al.*, 2004; *Pommrich et al.*, 2014] driven by the winds, temperature, and diabatic heating rates (vertical velocities) derived from this reanalysis. In the stratosphere and in the upper troposphere, potential temperature θ is employed as the vertical coordinate of the model and the cross-isentropic velocity $\dot{\theta} = Q$ is deduced from the ERA-Interim forecast total diabatic heating rates Q , including the effects of all-sky radiative heating, latent heat release, and diffusive heating [*Fueglistaler et al.*, 2009]. Both water vapor and ozone from CLaMS are compared with the Aura Microwave Limb Sounder (MLS) data, version 4.2, covering the period 2004–2013.

Using potential temperature as the vertical coordinate and ERA-Interim data, we reexamine in the next section the well-known features of the ENSO-related variability of the BD circulation [*Randel et al.*, 2009; *Calvo et al.*, 2010]. In sections 3 and 4, the zonally resolved analysis will be presented. Section 5 describes the slow vertical ascent of these anomalies into the tropical lower stratosphere (tape recorder) in the months following La Niña/El Niño winters and section 6 quantifies the zonal asymmetry due to ENSO. Finally, we discuss our results in section 7.

2. ENSO Anomaly of the BD Circulation

First, the reference DJF climatology of the BD circulation averaged over the 1979–2013 period is shown in Figure 1 (top row). Here the divergence of the EP flux, $\text{div}(\text{EPF})$ [*Andrews et al.*, 1987] (left) and the zonally averaged total diabatic heating rates $d\theta/dt$ (right) are displayed in a similar way as discussed in *Konopka et al.* [2015]. While $\text{div}(\text{EPF})$ measures the wave forcing of the residual circulation with negative values driving the poleward transport, $d\theta/dt$ quantifies the cross-isentropic transport with positive and negative values measuring upwelling and downwelling. The black contours are the climatological zonal winds with a clear signature of the subtropical jets and of the polar jet in the Northern Hemisphere above $\theta = 450$ K. The shallow and deep branches of the BD circulation can be clearly recognized in both diagnostics and are marked schematically as yellow arrows.

Historically, ENSO variability was mainly based on sea surface temperature (SST) anomalies exceeding a pre-selected threshold in a certain region of the equatorial Pacific [see, e.g., *Yeh et al.*, 2009, and references therein]. Here the ENSO variability is modeled in terms of the Multivariate ENSO Index (MEI) from the NOAA Climate Diagnostic Center, <http://www.esrl.noaa.gov/psd/enso/mei>, by using the method described in *Wolter* [1987].

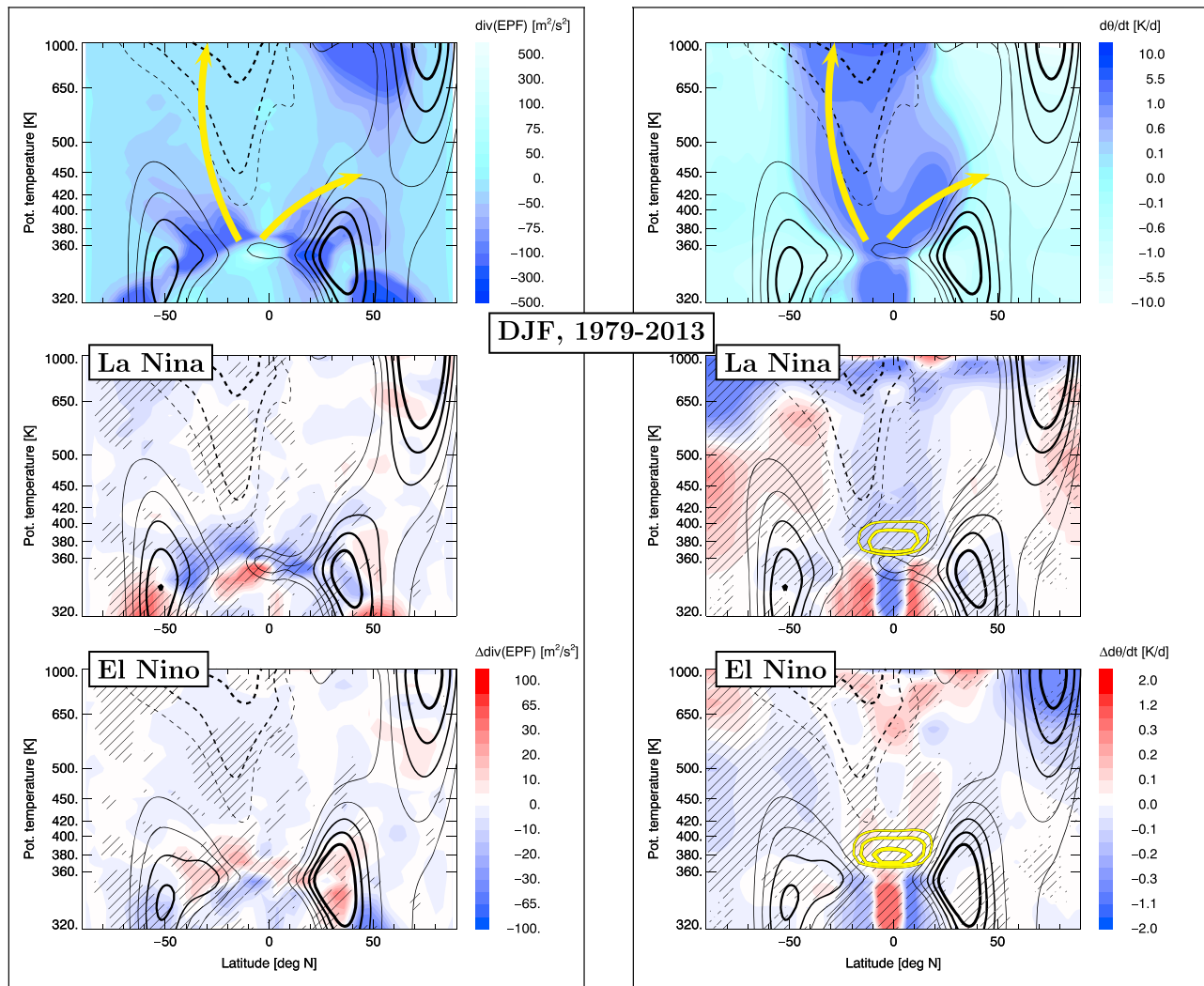


Figure 1. Zonally averaged view of the BD circulation during the La Niña/El Niño phases quantified in terms of the divergence of the Eliassen Palm flux (EPF), (left column) $\text{div}(\text{EPF})$ and of the zonally averaged total diabatic heating rates (right column) $d\theta/dt$ as derived from the ERA-Interim data. The $\text{div}(\text{EPF})$ quantifies the wave-induced force $(\bar{\sigma}a \cos \phi)^{-1} \nabla \cdot \vec{F}$ (see Andrews *et al.* [1987, equation 3.9.7a]; $\bar{\sigma}$ -isentropic zonal mean density, a -Earth's radius, ϕ -latitude). (top row) The 35 year DJF climatology (1979–2013). The solid and dashed lines are the zonal means of the westerlies (10, 15, 20, 25, and 30 m/s) and easterlies (-5 , -10 , -20 , and -30 m/s), respectively. (middle and bottom rows) Composites for the La Niña and El Niño winter months of the respective deseasonalized anomalies with statistically significant differences hatched. Zonal mean temperatures (yellow isolines with values 191, 193, and 195 K from thick to thin) and the total zonal wind averaged between 180 and 300°E are also shown.

MEI (Figure 2) is derived from a combination of SST and five other meteorological fields like surface wind, pressure, temperature, and total cloudiness.

Positive values of MEI quantify El Niño or warm ENSO events and correspond to warm SSTs in the tropical central Pacific (N3.4 region) as well as to warm tropical troposphere anomalies with enhanced zonal mean temperature at 300 hPa [Randel *et al.*, 2009]. On the other hand, La Niña or cold ENSO events are characterized by negative MEI values and are associated with a slightly colder SST and drier tropical troposphere. As we will see later, the strongest ENSO-related variability in the lower stratosphere is roughly confined to the region between $\pm 50^\circ\text{N}$ and between 180 and 300°E . In the following, we denote this region as the stratospheric ENSO region.

For almost all pronounced ENSO events the MEI peaks in late boreal fall, winter, and early spring. In the following, we define two sets (composites) of ENSO events by the condition $\text{MEI} < -0.9$ for La Niña and $\text{MEI} > 0.9$ for El Niño (red lines in Figure 2) and confine our analysis to the boreal winter season (DJF). The considered

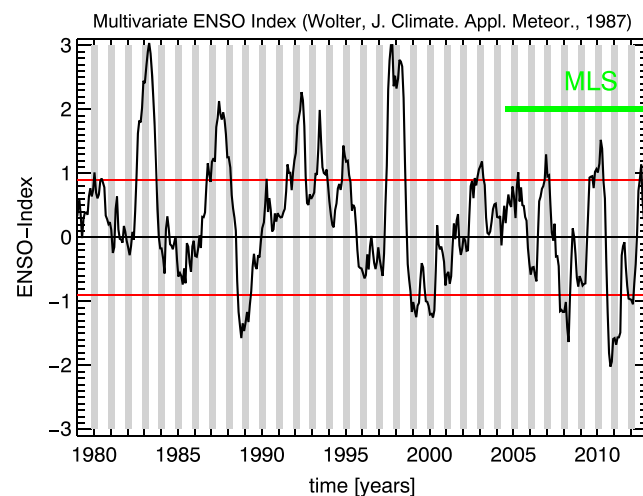


Figure 2. Multivariate ENSO Index (MEI) from the NOAA Climate Diagnostic Center, [Wolter, 1987; <http://www.esrl.noaa.gov/psd/enso/mei>]. The red lines denote the threshold values (± 0.9) defining the El Niño (positive) and La Niña (negative) composites as used in this paper. Gray shading shows DJF.

composites, also in relation to the QBO phase and to the mSSW as discussed in Tao *et al.* [2015], are listed in Table 1.

In this way we get statistically significant results both for the whole period 1979–2013 and for the 2004–2013 period where MLS data are available (17/27 and 8/5 winter month for the La Niña/El Niño cases during the whole period and the MLS period, respectively). Sensitivity studies by changing the threshold values by $\pm 10\%$, by extending the winter months (i.e., including November or March, like in Calvo *et al.* [2010]), or by removing 2 years with the westerly phase of the QBO in order to remove the QBO bias within the El Niño composite do not change our conclusions (we will come back to the last point in section 5).

Using these two subsets, the ENSO-related anomaly of the BD circulation can be quantified. First, the deseasonalized anomalies Δ are calculated, i.e., the mean annual cycle of the considered quantity calculated over the whole period 1979–2013 is subtracted from all elements of these two subsets. In Figure 1 (middle and bottom), such deseasonalized anomalies Δ of $\text{div}(\text{EPF})$ (left column) and of $d\theta/dt$ (right column) for the

Table 1. List of All Relevant La Niña (Boreal) Winters With MEI < -0.9 and El Niño Winters With MEI > 0.9 During the 1979–2013 Period^a

La Niña				El Niño			
Year	Months	QBO	mSSW	Year	Months	QBO	mSSW
1988/1989	DJF	W	X	1979/1980	D	E	X
1998/1999	DJF	E		1982/1983	DJF	W	
1999/2000	DJF	W	X	1986/1987	DJF	E	
2007/2008	DJF	E	X	1987/1988	DJ	W	X
2010/2011	DJF	W		1991/1992	DJF	E	
2011/2012	DJ	W/E	X	1992/1993	F	W	
				1994/1995	DJF	E/W	
				1997/1998	DJF	W	
				2002/2003	DJF	W	X
				2006/2007	DJ	W	
				2009/2010	DJF	E	X

^aIn total there are 17 and 27 winter months for the La Niña and El Niño composites, respectively, which are listed in the two main columns (D/J/F for December, January and February). In addition, the QBO phase (defined by 30 day smoothed equatorial wind at 50 hPa, E-easterly, W-westerly phase) and the winters with major Sudden Stratospheric Warmings (mSSW) as discussed in Tao *et al.* [2015] are marked with "X". Thus, within the La Niña (El Niño) composite there are 7 (11) months in the easterly phase and 10 (16) months in the westerly phase of the QBO.

La Niña and El Niño composites are shown. Statistically significant differences between these two composites (hatched, same for the following results) are found by using the Monte Carlo test with 95% confidence level and 1000 iteration steps. Remarkably, significant values of $\Delta \text{div}(\text{EPF})$ are confined to the region of the shallow branch of the BD circulation, i.e., to tropical and extratropical regions below $\theta = 400$ K. Note that the negative anomaly of $\text{div}(\text{EPF})$ during La Niña in the subtropics and tropics between 360 and 400 K leads to a deceleration of the westerlies and is accompanied by a slowdown of the tropical upwelling. Reversely, a positive anomaly of $\text{div}(\text{EPF})$ during El Niño seems to enhance tropical upwelling and, consequently, accelerates the BD circulation. Both anomalies of $\text{div}(\text{EPF})$ and $d\theta/dt$ are also consistent with the lowest zonal mean temperatures being colder during El Niño than during La Niña (yellow contours). The change of the globally integrated upward mass fluxes at 19 km is given by +9% during El Niño and -4% during La Niña phase, relative to the 1979–2013 DJF mean (not shown).

3. Zonally Resolved Impact of ENSO

In the previous section, we considered the ENSO-related anomaly of the BD circulation from a zonally averaged view. Thus, zonal asymmetries which may be expected from a spatially localized phenomenon like ENSO are lost by taking the zonal mean. To quantify the effect of eddy fluxes on the mean flow in terms of the EP flux, zonal averaging of correlation terms like $v'T'$ or $u'w'$ is a necessary step [(u, v, w) and T denote the 3-D wind and temperature, respectively, and primes define the deviations from the zonal means, see, e.g., Andrews *et al.* [1987]]. However, as proposed by Plumb [1985], all these (eddy) fluxes can be first averaged over time (here: over month or season) at every (longitude, latitude, altitude) grid point, i.e., before computing the zonal means (for some recent work on this topic, see Kinoshita and Sato [2013]). Plumb [1985] argues that in this way the stationary waves averaged over time (i.e., over month or season) can be regionally resolved in terms of a zonally resolved divergence of the EP flux.

Following the spirit of this approach, we start from the wave-induced force given by the divergence of the Eliassen-Palm flux vector $\bar{F} = (\bar{F}_\phi, \bar{F}_\theta)$ as $(\bar{\sigma}a \cos \phi)^{-1} \nabla \cdot \bar{F}$ and appearing on the right-hand side of the zonal mean zonal momentum equation in isentropic coordinates [see Andrews *et al.*, 1987, equation 3.9.7a]. Here $\bar{\sigma}$ is the isentropic zonal mean density of air, a the Earth's radius, ϕ latitude, and overlines denote the zonal average. To analyze the zonal contributions to this zonal mean force, we consider the three-dimensional terms contributing to the zonal mean divergence before calculating the longitudinal average. We denote these terms as 3-D horizontal EP flux divergence $F_{\text{hor}}^{\text{3D}} = (\sigma a \cos \phi)^{-1} \partial_\phi (F_\phi \cos \phi)$ and 3-D vertical EP flux divergence $F_{\text{vert}}^{\text{3D}} = \sigma^{-1} \partial_\theta F_\theta$, with [see Andrews *et al.*, 1987]

$$F_\phi = -a \cos \phi (\sigma v)' u' \quad (1)$$

$$F_\theta = g^{-1} p' \partial_\lambda M' - a \cos \phi (\sigma Q)' u' , \quad (2)$$

with λ longitude, g acceleration due to gravity, p pressure, Q the diabatic heating rate, and M the Montgomery stream function being the potential of geostrophic wind on the isentropic surface [see Andrews *et al.*, 1987]. We include the σ^{-1} factor in the definition of the divergence terms $F_{\text{hor}}^{\text{3D}}$ and $F_{\text{vert}}^{\text{3D}}$ for scaling reasons, as the force in the zonal momentum equation appears with this factor. Note that we do not consider additional terms in the zonal momentum equation which are not contributing to the zonal mean.

Following this procedure, in Figure 3 (top row) we show the boreal winter climatologies of temperature (left) and $\text{div}(\text{EPF}) := F_{\text{hor}}^{\text{3D}} + F_{\text{vert}}^{\text{3D}}$ at $\theta = 390$ K (right). Both quantities are derived from ERA-Interim data covering the winter months (DJF) from 1979 to 2013. Overlaid are respective horizontal winds and the isolines of the Montgomery stream function also marking the climatological structure of the horizontal wind. Note that the zonal integration of the zonally resolved $\text{div}(\text{EPF})$ exactly reproduces the zonal means shown in Figure 1 (top left).

While the horseshoe pattern of the lowest temperatures over the tropical Western Pacific with two almost symmetric anticyclones (Gill-Matsuno solution, see Gill [1980] and Matsuno [1966]) is a well-known feature of the boreal winter climatology [Nishimoto and Shiotani, 2012], the strongest meridional deviation of the horizontal wind from its mainly zonal direction can be diagnosed over the ENSO region. This indicates strong equatorial planetary wave activity in this region with subsequent eddy formation and dissipation. This wave-mean flow interaction is quantified in terms of the zonally resolved $\text{div}(\text{EPF})$ and shows the strongest negative signature in the ENSO region. Negative values (dark blue) decelerate and positive values (light blue) accelerate westerlies.

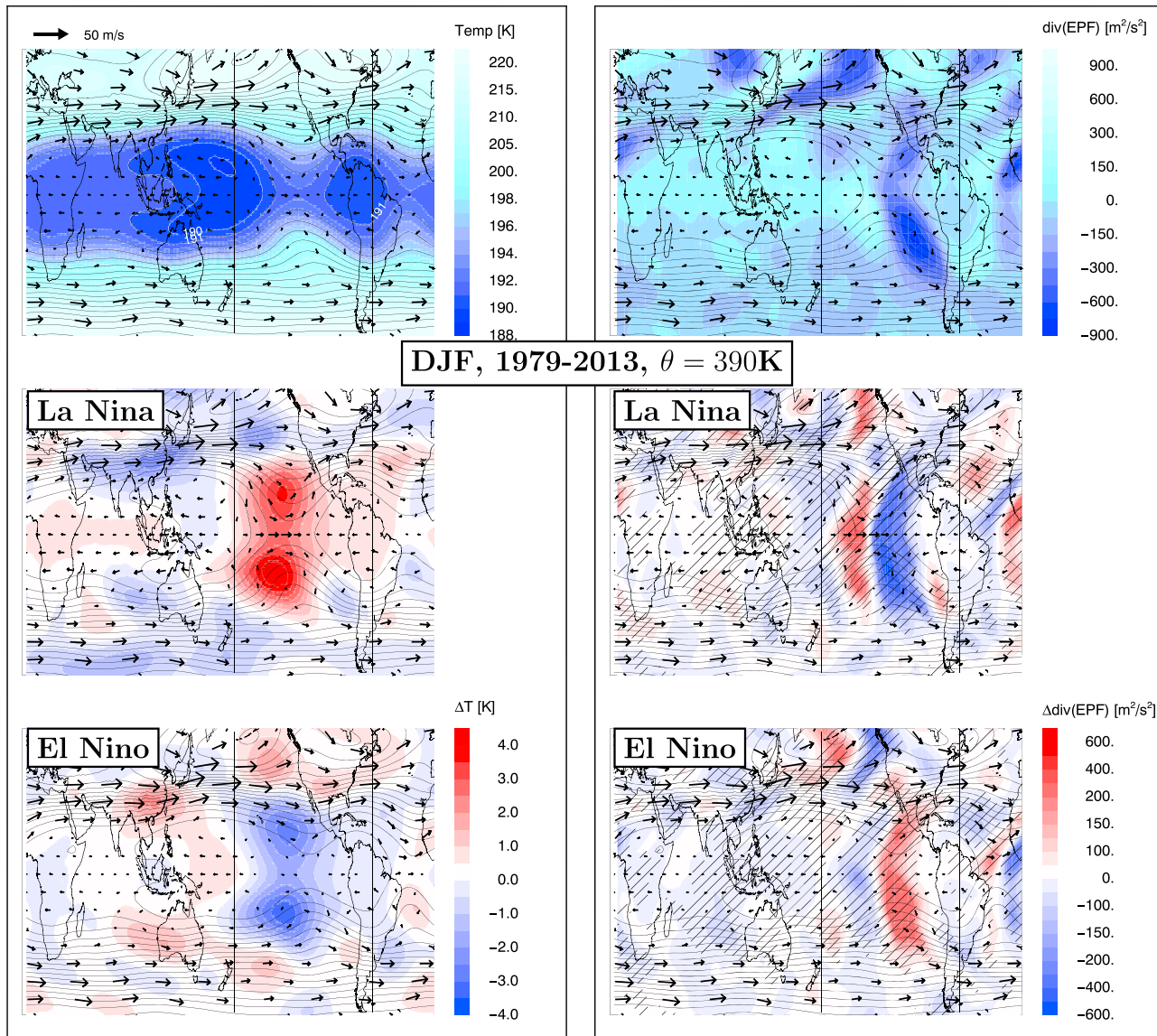


Figure 3. ENSO-related variability of temperature T and of the zonally resolved divergence of the EP flux $\text{div}(\text{EPF})$ at $\theta = 390$ K as derived from the ERA-Interim data. (top row) Absolute values averaged over the winter months (DJF) between 1979 and 2013. (middle and bottom rows) Composites of the deseasonalized anomalies Δ for the (left) La Niña and (right) El Niño winter months defined by the absolute values of ENSO index larger than 0.9. Overlaid are respective composites of horizontal wind and of the Montgomery stream function. All shown anomalies (i.e., ΔT values different from white color and hatched regions for $\Delta \text{div}(\text{EPF})$) are statistically significant differences between both composites.

Now we analyze the ENSO-related variability within this climatology. In Figure 3 (middle and bottom rows) the La Niña and El Niño composites of the deseasonalized anomalies are shown both for the temperature ΔT and for the zonally resolved $\Delta \text{div}(\text{EPF})$. Both patterns of ΔT and $\Delta \text{div}(\text{EPF})$ show strongest signatures within the ENSO region (i.e., between $\pm 50^\circ\text{N}$ and 180 to 300°E). Thus, during La Niña the lower stratosphere over the ENSO region is by ~ 4 K warmer and by ~ 4 K colder during El Niño if compared with the 35 year average. These anomalies are triggered by opposite anomalies in the troposphere with colder and warmer SSTs during La Niña and El Niño, respectively. Calvo et al. [2010] have shown that the cooling (warming) in the lowermost stratosphere is a dynamical response, mainly due to enhanced (reduced) gravity wave breaking that is a consequence of a strengthened (weakened) subtropical jet during El Niño (La Niña). However, the details of this coupling (due to direct influence of convection or due to wave-induced transport of heat from the tropics to the extratropics or because of both) are not completely clear, hitherto.

The analysis of the zonally resolved values of $\Delta \text{div}(\text{EPF})$ in the ENSO region implies that strong eddies decelerating and deforming westerlies can be diagnosed during La Niña, whereas during El Niño the mean flow becomes almost zonally aligned. This allows the interpretation that the upward propagating planetary waves are more strongly absorbed during La Niña than during El Niño. This enhanced wave-flow interaction process during La Niña phase is confined to the stratospheric ENSO region itself implying a more local forcing of the shallow branch of the BD circulation. However, a quantitative comparison with the effect of gravity waves as found by *Calvo et al.* [2010] still remains an open question.

4. ENSO Effect on Transport and Comparison With MLS

Clear climatological differences between a mean La Niña and El Niño state as discussed in Figure 3 for zonally resolved temperature, winds, $\text{div}(\text{EPF})$, and PV (not shown) distributions in the lower tropical stratosphere suggest that such differences should also be found between the respective zonally resolved distributions of water vapor, ozone, or mean age of air (AoA). Here we go beyond the zonal means discussed, e.g., in *Randel et al.* [2009] or *Calvo et al.* [2010] and discuss the regionally resolved patterns (see *Garfinkel et al.* [2013] for water vapor) as can be derived from the MLS observations and CLaMS simulations. Figures 4 and 5 show such La Niña/El Niño composites of deseasonalized anomalies of water vapor, $\Delta \text{H}_2\text{O}$, and of ozone, ΔO_3 , at $\theta = 390$ K as derived for the period 2004–2013 when MLS data (version 4.2) are available. Top rows show MLS observations, the middle rows the CLaMS results interpolated along the MLS profiles, and the bottom rows show the respective results from CLaMS for the whole ERA-Interim period (1979–2013). For $\Delta \text{H}_2\text{O}$, the isolines of lowest temperature at $\theta = 390$ K are overlaid, which are calculated for the same La Niña/El Niño ERA-Interim composites (i.e., extending over the 1979–2013 period) as estimates of the position of the (Lagrangian) cold point. The application of the MLS averaging kernels on CLaMS output does not significantly change the CLaMS distribution in low latitudes, so we show the “untreated” CLaMS output (as discussed in *Ploeger et al.* [2013], the strongest smoothing impact of the averaging kernel has to be expected for high latitudes rather than in the tropical lower stratosphere). The statistically significant differences between La Niña and El Niño composites are denoted as bold points.

The comparison between MLS and CLaMS composites of anomalies shows a remarkably good agreement although considerable differences exist between the absolute values (MLS water vapor and ozone in the tropics exceed CLaMS results by less than 0.3 ppmv and 100 ppbv, respectively, not shown). The comparison between the results for the MLS period (Figures 4 and 5, top and middle rows) with the results obtained for the whole ERA-Interim period (Figures 4, bottom row and 5, bottom row) also shows that the general features are the same, independent of the different time periods taken into account. While the dry water vapor anomaly during the El Niño phase can be found over the East Pacific and coincides well with the lowest temperatures in this region, the much weaker dry anomaly during the La Niña phase is located further west with respect to the temperature minimum (we will come back to this point in section 7). Moreover, the zonally resolved distributions are very different for the El Niño and La Niña cases with absolute differences exceeding 1 ppmv.

Finally, a supplementary picture of transport can be derived from the ozone anomalies shown in Figure 5. Lower (higher) ozone values in the tropics (extratropics) during El Niño are consistent with more upwelling (downwelling) in these regions if compared with La Niña. Due to mass conservation, an increased upwelling in the tropics (which is due to stronger wave activity in the extratropics as can be deduced from the El Niño panel in Figure 3) also results in an increased downwelling in the extratropics. Consequently, the enhanced downwelling in the extratropics brings in more ozone from higher latitudes/higher altitudes and could explain the extratropical enhancement of ozone during El Niño. On the other side, stronger eddy mixing during La Niña could also increase the two-way isentropic transport of ozone with a positive anomaly in the tropics and negative anomaly in the extratropics. By analyzing the ENSO-induced changes of the evolution of the mean age of air, we show in the next section that changes in the residual circulation outweigh those in eddy mixing, especially during El Niño.

5. Tape Recorder Signal of ENSO Anomalies

As shown in the previous section, La Niña and El Niño winters lead to very different horizontal patterns of H_2O or O_3 anomalies in the tropical and extratropical lower stratosphere. Figure 6 shows how these anomalies propagate upward during the months following the winter (DJF) season (tape recorder). The zonally

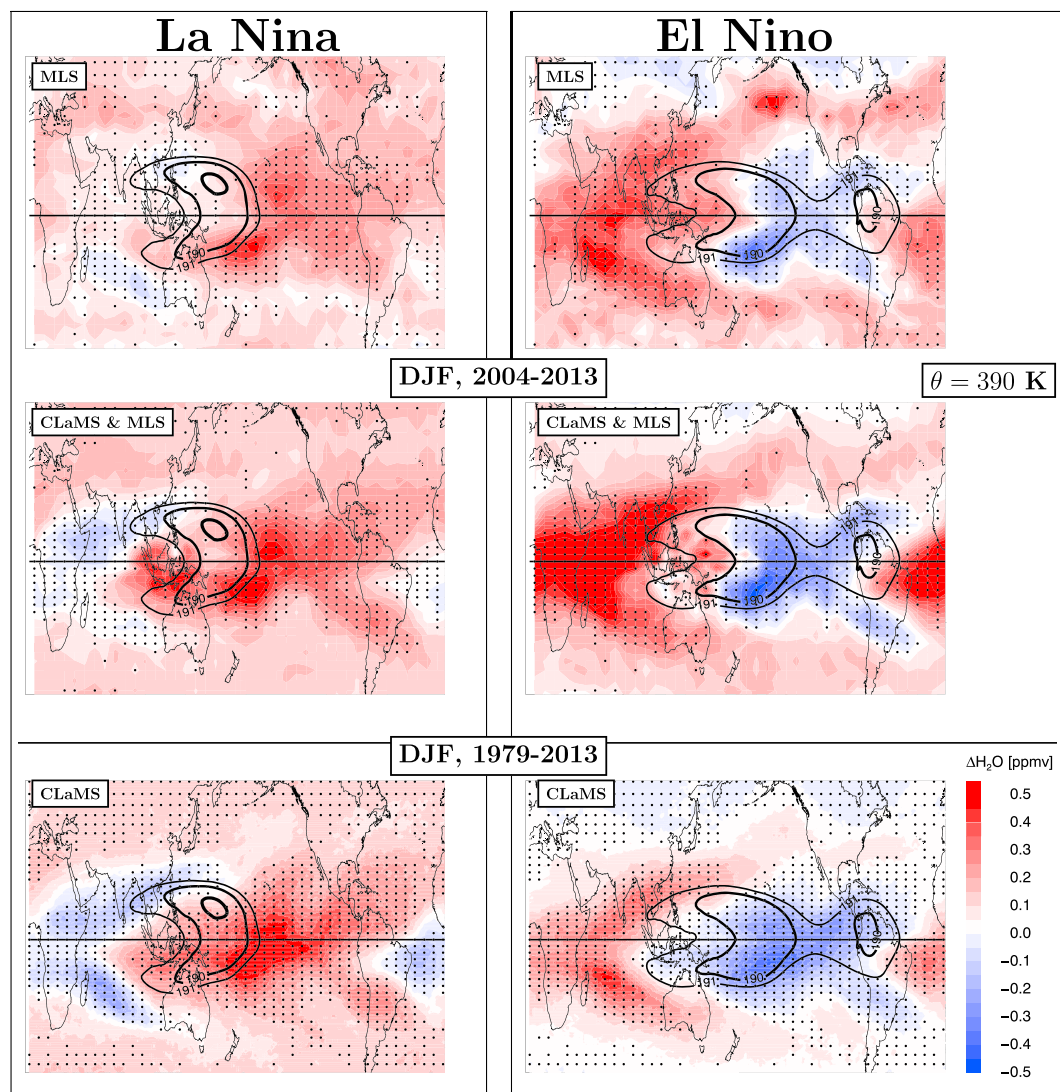


Figure 4. (top row) MLS water vapor (version 4.2) and (middle row) CLaMS water vapor sampled at the same times and locations as the MLS profiles at $\theta = 390$ K. Shown are La Niña/El Niño composites of respective deseasonalized anomalies calculated over winter months when MLS observations are available (2004–2013). (bottom row) Same type of composites but derived from CLaMS for the whole ERA-Interim period 1979–2013. Solid lines are isolines of the lowest temperatures found for these two composites between 1979 and 2013 (with values: 189, 190, and 191 K from thick to thin, respectively). Regions where the differences between La Niña and El Niño composites are statistically significant (at 95% confidence level) are marked with bold points.

and meridionally ($\pm 20^\circ\text{N}$) averaged signals are calculated for each of the 8 months following the respective La Niña/El Niño DJF season by using the same La Niña/El Niño composites as in the previous sections. For example, the data 4 months after a December with $\text{MEI} > 0.9$ and the data 4 months after a February with $\text{MEI} > 0.9$ are collected within the same time bin, i.e., within the fourth month bin after the ENSO winter. In this way, the effect of ENSO on the air composition during the months following the ENSO winter can be investigated.

Figure 6 shows results for water vapor and ozone as observed by MLS and simulated with CLaMS along the MLS profiles. Black dots denote statistically significant results, and the thick solid gray line in the water vapor plots approximates the mean position of the absolute water vapor maximum, i.e., of the “true” water vapor tape recorder as derived from the MLS observations (2004–2013). While a clear wet anomaly propagates upward to about $\theta = 600$ K around 7 months after the (warm tropospheric) El Niño winter, a slightly weaker reverse pattern can be diagnosed following La Niña. The upward velocity of this propagation is roughly the same as

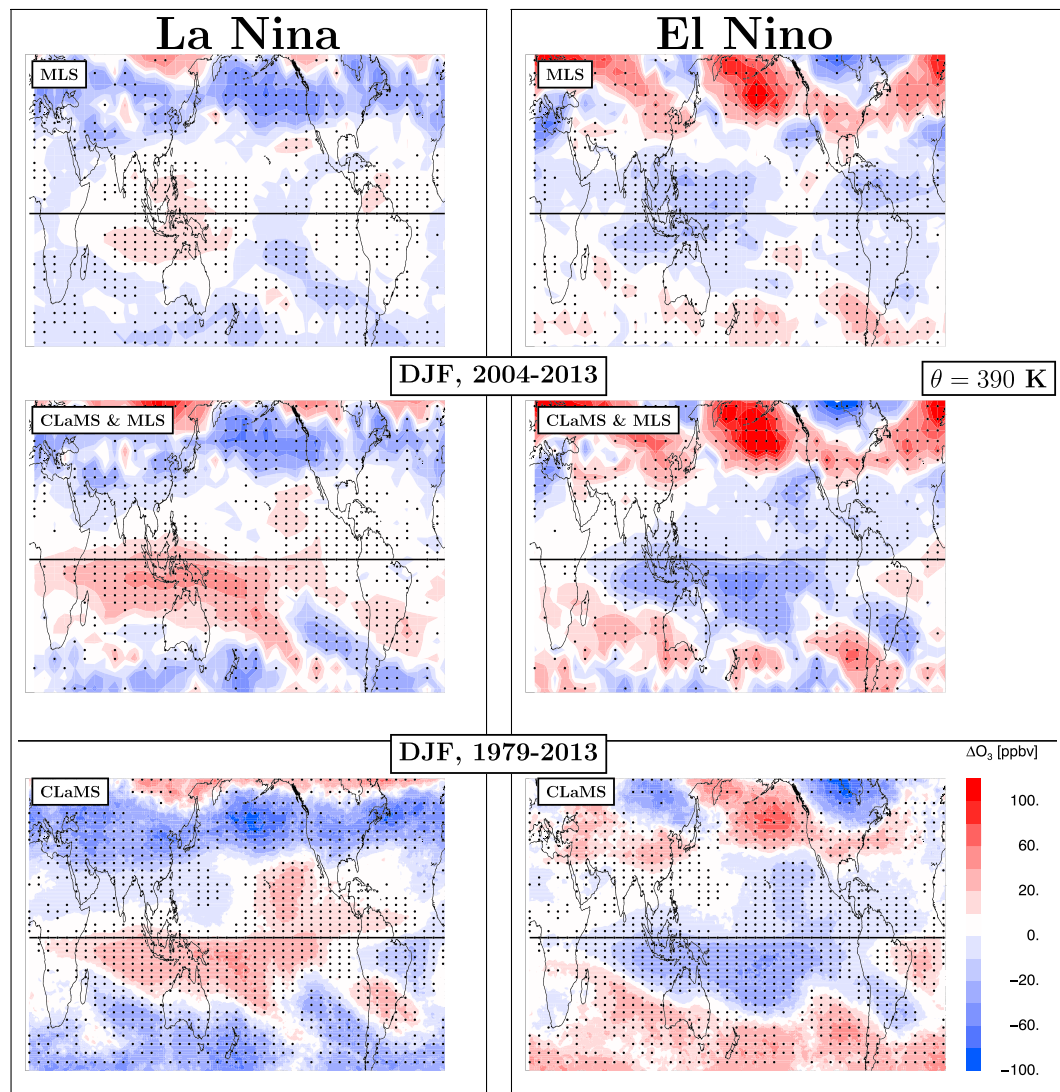


Figure 5. Same as Figure 4 but for ozone.

that of the “true” water vapor tape recorder. CLaMS simulations along MLS profiles reproduce the observed patterns well. A slightly faster upward propagation of the tape recorder signal in CLaMS is consistent with the low temperature bias and, consequently, faster upwelling in the ERA-Interim data [Dee et al., 2011].

While the signature of the water vapor anomaly originates at the tropical tropopause and propagates upward, the reasons for the ozone anomalies are different. First, we should notice that while water vapor in CLaMS is calculated within the whole stratosphere, ozone above $\theta = 500$ K is prescribed by the climatology [Pommrich et al., 2014] which gives the reason for a strong discrepancy between the model and MLS observations in this region. Second, because ozone lifetime is shorter than that of water vapor, we are seeing a cumulative effect of transport and chemistry for ozone, while for water only transport influences the signal which was set at the coldest temperature a parcel encountered. Thus, a negative ozone anomaly after El Niño winter seems to be consistent with a stronger upwelling during El Niño [Randel et al., 2009; Calvo et al., 2010]. However, this could also be caused by less in-mixing from the extratropics into the tropics as recently discussed by Ploeger et al. [2015a] (we will come to this point later on).

To complete the picture and make our analysis statistically robust, Figure 7 shows the same type of diagnostic but for the whole period 1979–2013. Instead of ozone, mean age of air (AoA) is shown in Figure 7 (bottom), which allows clearer statements with respect to transport if compared with a chemically active tracer like ozone. Once again, the tape recorder pattern of the ENSO-related water vapor anomalies is almost the same

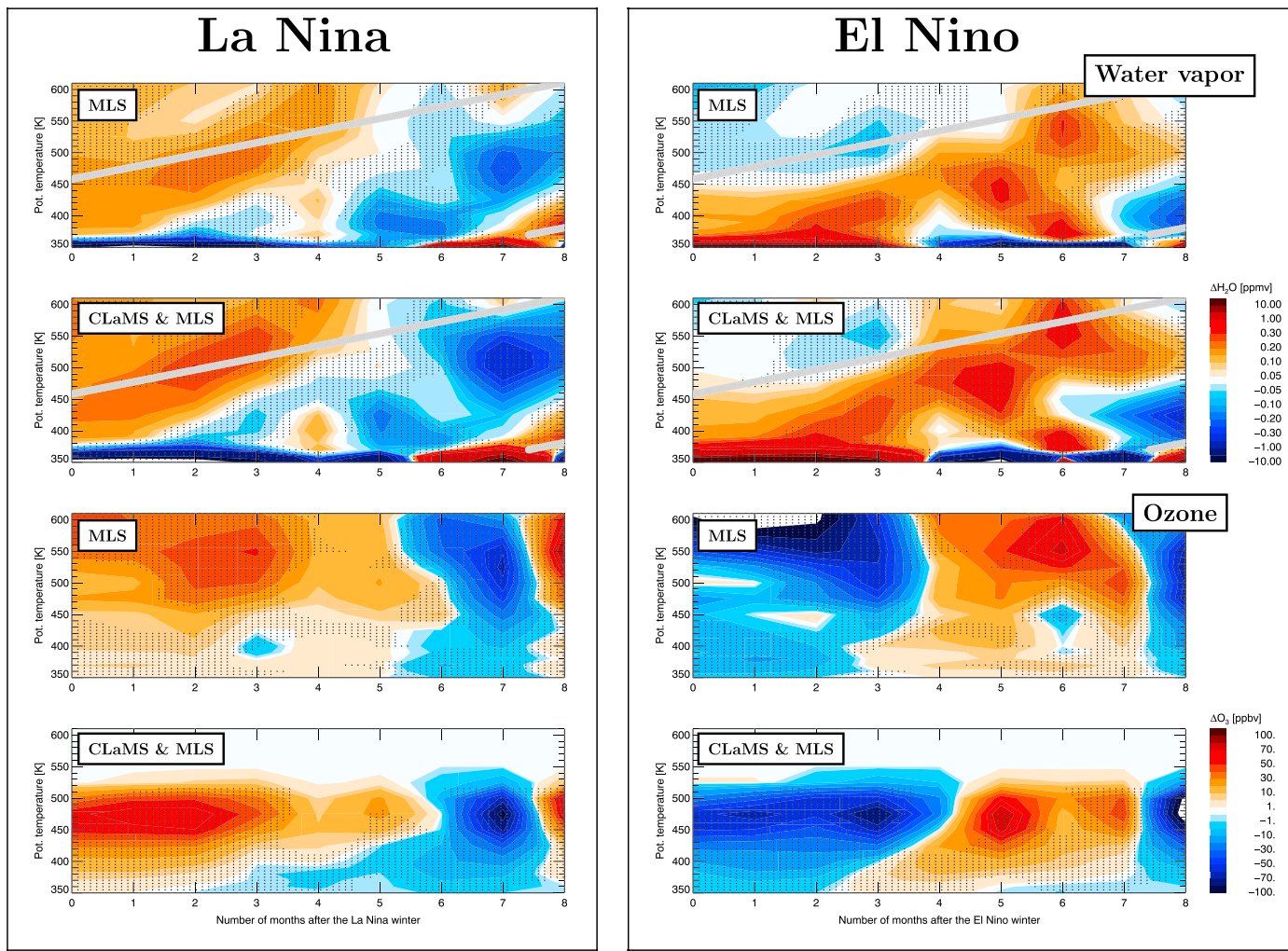


Figure 6. (first and second rows) Water vapor tape recorder signal ($\pm 20^\circ\text{N}$) of the deseasonalized ENSO anomaly calculated for the months following the (left) La Niña and the (right) El Niño winters by using the same type of composites as in the previous sections. The zero mark denotes the middle of the DJF season (i.e., 15 January). In the first and second rows MLS observations and CLaMS results interpolated along the MLS profiles are shown. (third and fourth rows) Same as first and second rows but for ozone. Black dots mark statistically significant regions. The thick solid gray line in the water vapor plots approximates the mean position of the absolute water vapor maximum, i.e., of the “true” water vapor tape recorder as derived from the MLS observations (2004–2013).

as in Figure 6, albeit slightly weaker, with stratospheric differences of about 0.2–0.3 ppmv between 2 and 8 months after El Niño and of about 0.1–0.2 ppmv after La Niña winters. These results are robust if the considered composites are slightly changed in order to remove a potential bias regarding the QBO phase. As can be seen from Table 1, La Niña winters are almost equally affected by westerly and easterly QBO phases, while during El Niño the westerly QBO phase is overrepresented. However, by removing 4 years with the influence of the westerly QBO (1997/1998 and 2002/2003), the change of stratospheric water entry values is less than 5%. On the other hand, the tape recorder pattern becomes slightly faster and more pronounced (by ≈ 0.1 ppmv) being consistent with faster upwelling during the easterly QBO phase.

Furthermore, the signatures of AoA are different although more similar to the distribution of ozone shown in Figure 6 (bottom). The most striking feature is that in the first 4–5 months after El Niño (La Niña), wet (dry) H_2O anomaly is related to younger (older) AoA. However, this relationship is much less pronounced after La Niña winters, although the ΔAoA signatures of the La Niña and El Niño composites are strongly anticorrelated.

Nevertheless, the anomalies diagnosed in the AoA allow a much clearer interpretation. Using a Lagrangian reconstruction of AoA along the residual circulation trajectories [see Ploeger *et al.*, 2015b], Figure 8 decomposes the ENSO-related anomaly of ΔAoA into the contributions of the residual circulation (Figure 8, top) and

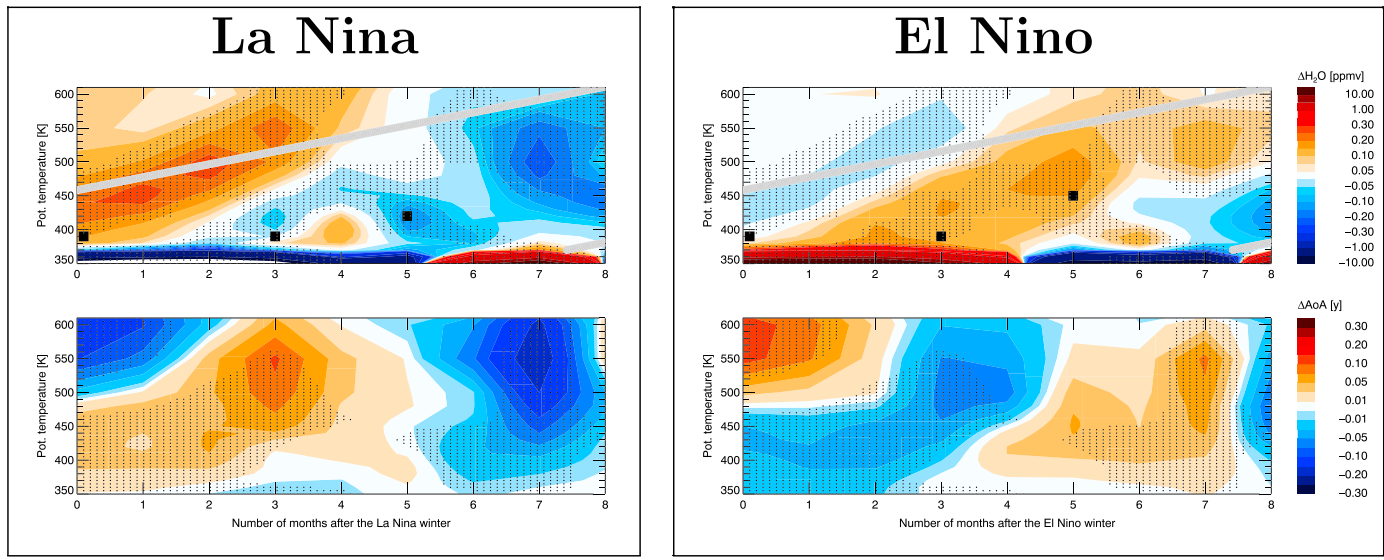


Figure 7. (top row) ENSO-related water vapor tape recorder anomaly as in Figure 6 but from the whole CLaMS simulation covering the period 1979–2013. The zonally resolved distributions at the positions denoted by black squares are discussed in Figure 11. (bottom row) Same as Figure 7 (top row) but for the mean age of air (AoA).

of eddy mixing (Figure 8, middle). The quality of this decomposition is shown in Figure 8 (bottom) where the total sum of ΔAoA (i.e., residual circulation + eddy mixing) is shown with only small differences to the original ΔAoA distribution (Figure 7, bottom). We conclude that differences in ΔAoA due to residual circulation (stronger during El Niño) dominate the differences due to eddy mixing, with respective contributions given by 2/3 for residual circulation and 1/3 for eddy mixing. Especially during El Niño, planetary waves are less

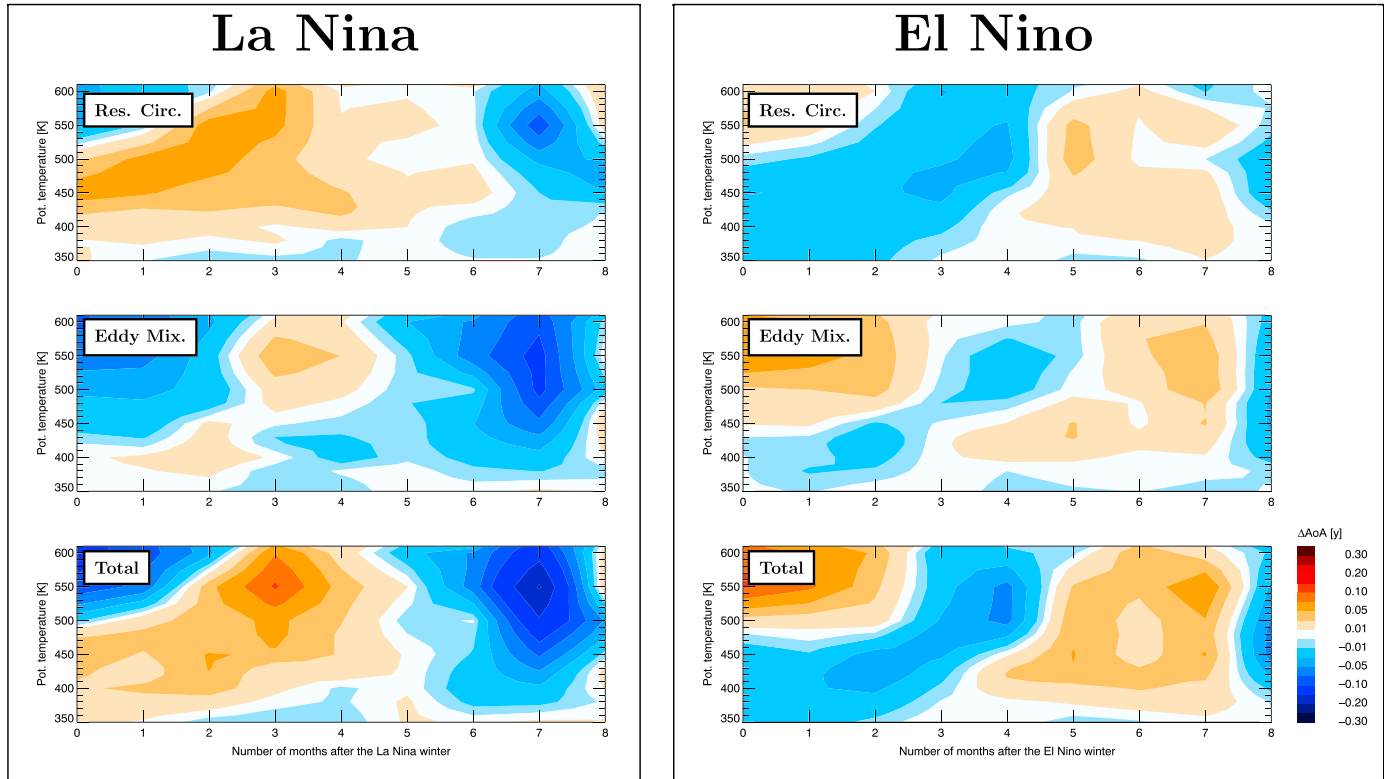


Figure 8. Decomposition of ΔAoA into the contributions of the residual circulation (transit time along the 2-D residual circulation trajectories, top) and of eddy mixing (integrated mixing along the trajectories, middle). (bottom) The total sum of ΔAoA (i.e., residual circulation + eddy mixing) is shown [Ploeger et al., 2015b].

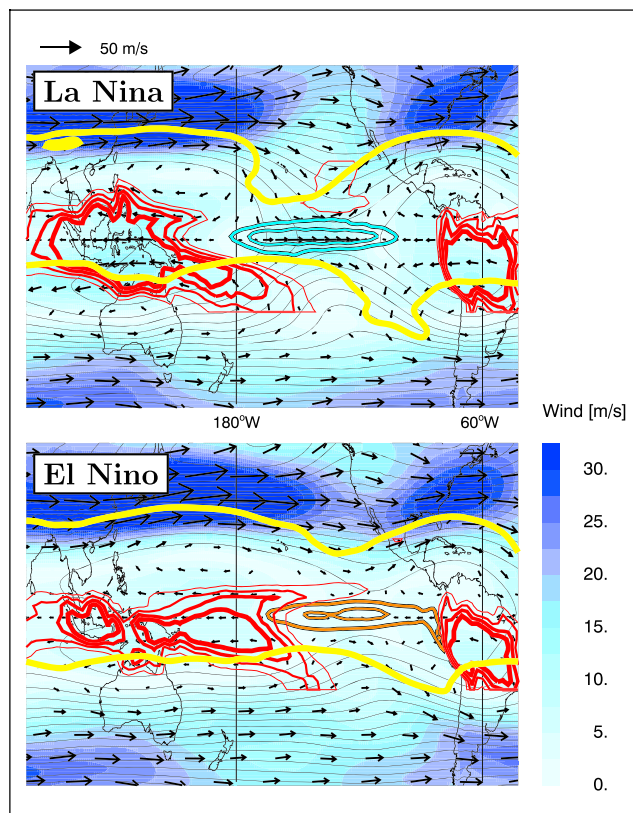


Figure 9. Climatological horizontal wind (color bar and arrows), PV = 5 PVU line (yellow) and Montgomery stream function (black lines) distributions at $\theta = 390$ K for the La Niña/El Niño cases. In addition, the SST anomalies as derived from the lowest ERA-Interim layer are the proxies for regions with enhanced ENSO variability (orange, El Niño/cyan, La Niña for positive/negative anomaly with isolines for ± 1 and ± 1.5 K, respectively). Furthermore, the respective OLR climatology is shown quantifying the anomalies of the convective activity (red, 210, 220, 230, and 240 W/m^2 from thick to thin).

absorbed by the meandering jets and break at higher altitudes causing a faster tropical upwelling that is consistent with a younger AoA anomaly in the deep tropics and with less (more) ozone in the tropics (extratropics) as discussed in Figure 5.

6. ENSO and the Zonal Asymmetry

These different patterns of wave dissipation seem also to be related to different patterns of sea surface temperature (SST) and convection which strongly influence the ENSO variability. Figure 9 shows properties of the flow in the lower tropical stratosphere centered over the Pacific as derived from ERA-Interim. Here the total horizontal wind (color coded) as well as the PV isolines ($\text{PV} = 5 \text{ PVU}$, yellow) depict the differences between La Niña and El Niño configurations. Furthermore, as a proxy for the climatological position of convection, regions with low Outgoing Longwave Radiation (OLR) are highlighted by red isolines. This satellite-based climatology is derived from the NOAA interpolated OLR data between 1979 and 2013, <http://www.esrl.noaa.gov/psd/enso/mei>, and by using the same composites of La Niña/El Niño events as in our previous analysis. Finally, the respective proxy for the SST anomaly (cyan/orange-negative/positive anomaly during La Niña/El Niño) is derived from the lowest layer of the ERA-Interim data.

Both the absolute values of the horizontal wind as well as its direction indicate that during the El Niño winters the convection extends to the Eastern Pacific and the winds become more zonally symmetric, especially in the northern extratropics, east of the 180°E meridian, if compared with the La Niña situation. Consistently, the PV distribution (here $\text{PV} = 5 \text{ PVU}$ isoline, yellow) during La Niña shows a stronger stratospheric influence in this region indicating enhanced isentropic mixing. At the lower levels, such stratospheric intrusions coincide with

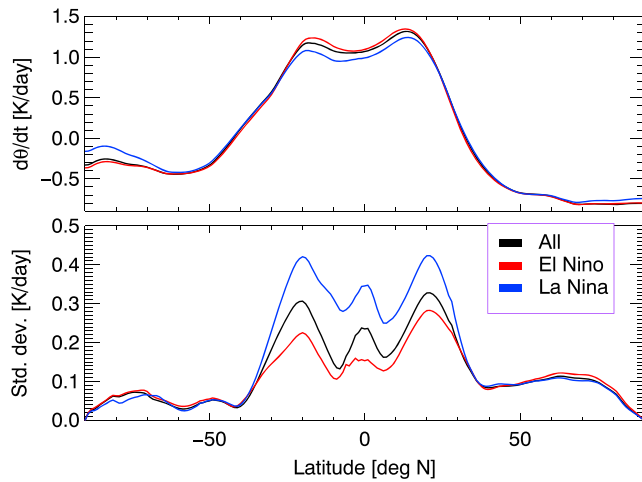


Figure 10. Zonally averaged diabatic vertical velocities at $\theta = 390$ K and the respective standard deviation for all boreal winters (DJF) between 1979 and 2013 as well for the La Niña/El Niño composites. The enhanced standard deviation relative to the zonal mean in the tropics during La Niña phase has its origin in the enhanced zonal variability of the subtropical jets, mainly in the ENSO region.

regions of westerly tropical winds over the Western Pacific, so-called “westerly ducts” [Waugh and Polvani, 2000]. Waugh and Polvani [2000] also found a strong interannual variability of such events, with fewer events during El Niño.

These findings are also consistent with recent results of an idealized aqua planet study. Yang *et al.* [2014] found that the zonal distribution of SST perturbations has a major impact on the vertical and meridional structure of the BD circulation. Zonally localized SST heating (like during La Niña) tends to generate a shallow acceleration of the stratospheric residual circulation and enhanced isentropic mixing associated with a weakened stratospheric jet. In contrast, SST heating with a zonally symmetric structure (like during El Niño) tends to produce a deep strengthening of the stratospheric residual circulation, suppressed isentropic mixing associated with a stronger stratospheric jet, and a decrease of AoA in the entire stratosphere. Yang *et al.* [2014] also linked the shallow versus deep strengthening of the stratospheric residual circulation to wave propagation and dissipation in the subtropical lower stratosphere rather than wave generation in the troposphere.

To quantify the ENSO-related zonal asymmetry of the BD-circulation, Figure 10 shows the zonally averaged diabatic vertical velocities $d\theta/dt$ at $\theta = 390$ K and the respective standard deviation for all boreal winters (DJF) between 1979 and 2013 as well as for the La Niña/El Niño composites. As expected, largest and smallest absolute values of $d\theta/dt$ could be diagnosed for El Niño and La Niña cases, respectively. Interestingly, the standard deviation in the tropics is almost twice as large during La Niña relative to El Niño and has its origin in the enhanced zonal and meridional variability of the northern hemispheric subtropical jet between 180 and 300°E. Furthermore, this increase in zonal asymmetry at $\theta = 390$ K is mostly confined to the tropics and negligible in high latitudes.

7. Discussion and Conclusions

A particularly remarkable result concerns the zonally averaged ENSO anomalies of water vapor transport into the lower tropical stratosphere with wet (dry) anomalies following the El Niño (La Niña) winters (see water vapor tape recorder signatures in Figures 6 and 7). However, as can be inferred from Figure 4 (bottom), the water vapor during La Niña at $\theta = 390$ K shows mostly positive anomalies apparently contradicting the expected dry anomaly of the zonal mean after the La Niña winter. To resolve this contradiction, Figure 11 shows the zonally resolved view after 3 (top row) and 5 (bottom row) months for $\theta = 390$ K (top row) and for $\theta = 420/450$ K (bottom row) for the La Niña/El Niño composites, respectively. The corresponding positions in the tape recorder plots (Figure 7) are denoted as black squares. First, the anomalies during the ENSO winter are mainly caused by temperature anomalies at the tropical tropopause, i.e., in the θ range between 370 and 380 K. Thus, to see this effect at $\theta = 390$ K, we have to move in time by an appropriate time lag, here by 3 and 5 months in Figures 11 (top) and 11 (bottom), respectively. From these plots it is not only obvious how the dry

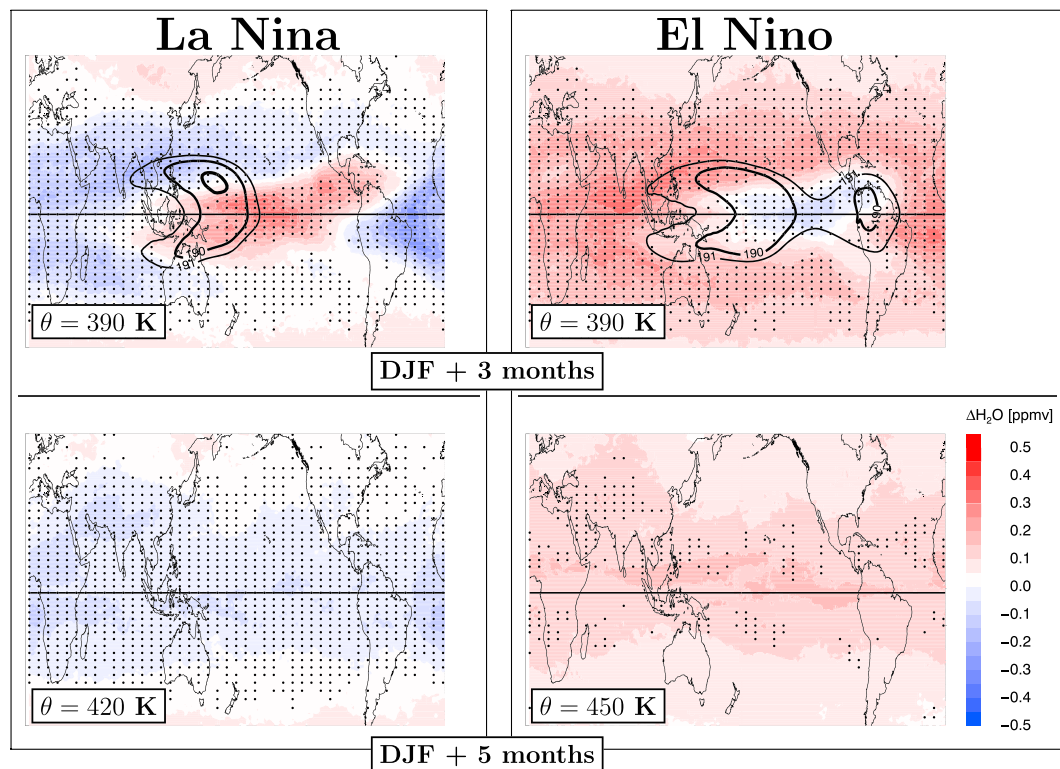


Figure 11. Zonally resolved CLaMS composites of water vapor for (top) 3 and (bottom) 5 months after the ENSO event shown in the same way as in Figure 4 (bottom). (top row) The $\theta = 390$ K is used with the same lowest temperatures isolines (black) as in Figure 4. To take into account the ascending of the tape recorder anomaly, (bottom row) CLaMS composites shifted by 5 months are shown at $\theta = 420$ K and 450 K, for the La Niña/El Niño composites, respectively (compare with black squares in Figure 7).

and wet anomalies evolve during the months following the respective ENSO phase but we can also see how the zonally inhomogeneous imprints of water vapor anomalies homogenize along the zonal direction with time and altitude as they propagate upward into the stratosphere. Because the El Niño anomaly propagates slightly faster than the La Niña signal, we choose two different potential temperatures, $\theta = 450$ and 420 K, respectively, to catch these anomalies after 5 months of upward transport.

Furthermore, although during El Niño winters, a stronger residual circulation coincides with lowest mean temperatures in the TTL, this fact does not necessarily mean that freeze drying in the coldest regions of the TTL is more efficient than during La Niña. Our analysis rather shows the opposite, i.e., a dry anomaly following La Niña winters. The reasons for this puzzling fact are different signatures in the local (Lagrangian) cold points and the temperature zonal means [Holton and Gettelman, 2001; Bonazzola and Haynes, 2004]. This can be seen by comparing the respective zonal means of the lowest temperatures in Figure 1 (yellow isolines) with the horizontal temperature distribution at $\theta = 390$ K in Figure 4 (black isolines) being a proxy for the Lagrangian cold point. Thus, the (absolute) lowest temperatures can be diagnosed during La Niña phase whereas the lowest zonal mean temperatures can obviously be found during El Niño. However, while the differences of H_2O in the zonally resolved picture are of the order 1 ppmv, these differences become much smaller for the zonal mean and are of the order 0.2 ppmv. The tape recorder structure of these anomalies which ascend into the lower tropical stratosphere is a very robust signature if the meridional range is changed from ± 10 to $\pm 25^\circ N$.

El Niño and La Niña define two different states of atmospheric dynamics and composition extending into the lower stratosphere. The strong zonal asymmetry of water vapor, ozone, or EP flux distributions during La Niña is contrasted with much more zonally symmetric distributions during El Niño. The asymmetry between El Niño and La Niña is strongest in the tropics and much weaker at high latitudes. Therefore, the zonally symmetric picture of the residual circulation, in particular, of the climatological variability of tropical upwelling at the lower levels of the stratosphere, needs a more longitudinally resolved description, especially during strong La Niña years.

Based on comparison of different meteorological reanalysis products, *Abalos et al.* [2015] found that changes in the global BD circulation are mainly linked to the boreal winter season during which ENSO variability peaks. Zonal differences between the mean El Niño and La Niña states around the cold point tropical tropopause may have an impact on regional climate variability, the pathway of water vapor into the stratosphere and, consequently on climate trends. In particular, very low temperatures in this region strongly influence the radiation escaping the troposphere into space and trace gas changes in this region are therefore likely to affect surface climate [*Gettelman et al.*, 2011; *Riese et al.*, 2012].

Finally, although we are in agreement with previous studies that strong El Niño (La Niña) events moisten (dry) the stratosphere, their interaction with the mSSW as discussed in *Tao et al.* [2015], which mainly dry the stratosphere, especially during the easterly QBO phase, is still an open question. In our study, the mSSWs occur with similar frequency for the considered El Niño/La Niña composites (see Table 1) and, presumably, their effects cancel. However, their interaction with ENSO variability cannot be excluded mainly because of a limited length of our time series (35 years). Longer time series as provided by climate models are needed to find a possible connection.

Acknowledgments

The European Centre for Medium-Range Weather Forecasts (ECMWF) provided meteorological analysis for this study (ERA-Interim). These data are free, available from the ECMWF WEB page: http://data-portal.ecmwf.int/data/d/interim_daily/. The Aura Microwave Limb Sounder (MLS) data, version 4.2, covering the period 2004–2013 are free, available from the WEB page: <http://mls.jpl.nasa.gov/>. The CLaMS model data may be requested from the corresponding author (p.konopka@fz-juelich.de). Excellent programming support was provided by N. Thomas. The authors sincerely thank Rolf Müller for helpful discussions. Finally, we would like to thank all three reviewers for their insightful and probably very time-consuming comments on the paper, as these comments led us to an improvement of the work.

References

- Abalos, M., B. Legras, F. Ploeger, and W. J. Randel (2015), Evaluating the advective Brewer-Dobson circulation in three reanalyses for the period 1979–2012, *J. Geophys. Res. Atmos.*, **120**, 7534–7554, doi:10.1002/2015JD023182.
- Andrews, D. G., J. R. Holton, and C. B. Leovy (1987), *Middle Atmosphere Dynamics*, 489 pp., Academic Press, San Diego, Calif.
- Baldwin, M., et al. (2001), The quasi-biennial oscillation, *Rev. Geophys.*, **39**(2), 179–229.
- Bonazzola, M., and P. H. Haynes (2004), A trajectory-based study of the tropical tropopause region, *J. Geophys. Res.*, **109**, D20112, doi:10.1029/2003JD004356.
- Calvo, N., R. R. Garcia, W. J. Randel, and D. Marsh (2010), Dynamical mechanism for the increase in tropical upwelling in the lowermost tropical stratosphere during warm ENSO events, *J. Atmos. Sci.*, **67**(7), 2331–2340, doi:10.1175/2010JAS3433.1.
- Calvo-Fernandez, N., R. R. Garcia, R. Garcia Herrera, D. Gallego Puyol, L. Gimeno Presa, E. Hernandez Martin, and P. Ribera Rodriguez (2004), Analysis of the ENSO signal in tropospheric and stratospheric temperatures observed by MSU, 1979–2000, *J. Clim.*, **17**, 3934–3946, doi:10.1175/1520-0442(2004)017.
- Dee, D. P., et al. (2011), The ERA-Interim reanalysis: Configuration and performance of the data assimilation system, *Q. J. R. Meteorol. Soc.*, **137**, 553–597, doi:10.1002/qj.828.
- Dessler, A., M. Schoeberl, T. Wang, S. Davis, and K. Rosenlof (2013), Stratospheric water vapor feedback, *Proc. Natl. Acad. Sci. U.S.A.*, **110**(45), 18,087–18,091, doi:10.1073/pnas.1310344110.
- Fueglistaler, S., and P. H. Haynes (2005), Control of interannual and longer-term variability of stratospheric water vapor, *J. Geophys. Res.*, **110**, D24108, doi:10.1029/2005JD006019.
- Fueglistaler, S., B. Legras, A. Beljaars, J.-J. Morcrette, A. Simmons, A. M. Tompkins, and S. Uppapla (2009), The diabatic heat budget of the upper troposphere and lower/mid stratosphere in ECMWF reanalyses, *Q. J. R. Meteorol. Soc.*, **135**(638), 21–37, doi:10.1002/qj.361.
- Garfinkel, C. I., M. M. Hurwitz, L. D. Oman, and D. W. Waugh (2013), Contrasting effects of Central Pacific and Eastern Pacific El Niño on stratospheric water vapor, *Geophys. Res. Lett.*, **40**, 4115–4120, doi:10.1002/grl.50677.
- Geller, M. A., X. L. Zhou, and M. H. Zhang (2002), Simulations of the interannual variability of stratospheric water vapor, *J. Atmos. Sci.*, **59**, 1076–1085.
- Gettelman, A., P. Hoor, L. L. Pan, W. J. Randel, M. I. Hegglin, and T. Birner (2011), The extratropical upper troposphere and lower stratosphere, *Rev. Geophys.*, **49**, RG3003, doi:10.1029/2011RG000355.
- Gill, A. E. (1980), Some simple solutions for heat-induced tropical circulation, *Q. J. R. Meteorol. Soc.*, **106**, 447–462.
- Hegglin, M. I., et al. (2014), Vertical structure of stratospheric water vapour trends derived from merged satellite data, *Nat. Geosci.*, **7**, 768–776, doi:10.1038/Ngeo2236.
- Holton, J. R., and A. Gettelman (2001), Horizontal transport and the dehydration of the stratosphere, *Geophys. Res. Lett.*, **28**(14), 2799–2802.
- Kinoshita, T., and K. Sato (2013), A formulation of three-dimensional residual mean flow applicable to both inertia-gravity waves and to Rossby waves, *J. Atmos. Sci.*, **70**, 1577–1602, doi:10.1175/JAS-D-12-0137.1.
- Konopka, P., et al. (2004), Mixing and ozone loss in the 1999–2000 Arctic vortex: Simulations with the 3-dimensional Chemical Lagrangian Model of the Stratosphere (CLaMS), *J. Geophys. Res.*, **109**, D02315, doi:10.1029/2003JD003792.
- Konopka, P., F. Ploeger, M. Tao, T. Birner, and M. Riese (2015), Hemispheric asymmetries and seasonality of mean age of air in the lower stratosphere: Deep versus shallow branch of the Brewer-Dobson circulation, *J. Geophys. Res. Atmos.*, **120**, 2053–2066, doi:10.1002/2014JD022429.
- Krüger, K., S. Tegtmeier, and M. Rex (2008), Long-term climatology of air mass transport through the Tropical Tropopause Layer (TTL) during NH winter, *Atmos. Chem. Phys.*, **8**, 813–823.
- Liess, S., and M. A. Geller (2012), On the relationship between QBO and distribution of tropical deep convection, *J. Geophys. Res.*, **117**, D03108, doi:10.1029/2011JD016317.
- Matsuno, T. (1966), Quasi-geostrophic motions in the equatorial area, *J. Meteorol. Soc. Jpn.*, **44**(1), 25–42.
- McKenna, D. S., P. Konopka, J.-U. Grooß, G. Günther, R. Müller, R. Spang, D. Offermann, and Y. Orsolini (2002), A new Chemical Lagrangian Model of the Stratosphere (CLaMS): 1. Formulation of advection and mixing, *J. Geophys. Res.*, **107**(D16), 4309, doi:10.1029/2000JD000114.
- Nishimoto, E., and M. Shiotani (2012), Seasonal and interannual variability in the temperature structure around the tropical tropopause and its relationship with convective activities, *J. Geophys. Res.*, **103**, D02104, doi:10.1029/2011JD016936.
- Ploeger, F., G. Günther, P. Konopka, S. Fueglistaler, R. Müller, C. Hoppe, A. Kunz, R. Spang, J.-U. Grooß, and M. Riese (2013), Horizontal water vapor transport in the lower stratosphere from subtropics to high latitudes during boreal summer, *J. Geophys. Res. Atmos.*, **118**, 8111–8127, doi:10.1002/jgrd.50636.
- Ploeger, F., M. Riese, F. Haenel, P. Konopka, R. Müller, and G. Stiller (2015a), Variability of stratospheric mean age of air and of the local effects of residual circulation and eddy mixing, *J. Geophys. Res. Atmos.*, **120**, 716–733, doi:10.1002/2014JD022468.

- Ploeger, F., M. Abalos, T. Birner, P. Konopka, B. Legras, R. Müller, and M. Riese (2015b), Quantifying the effects of mixing and residual circulation on trends of stratospheric mean age of air, *Geophys. Res. Lett.*, 42, 2047–2054, doi:10.1002/2014GL062927.
- Plumb, R. A. (1985), On the three-dimensional propagation of stationary waves, *J. Atmos. Sci.*, 42, 217–229.
- Pommrich, R., et al. (2014), Tropical troposphere to stratosphere transport of carbon monoxide and long-lived trace species in the Chemical Lagrangian Model of the Stratosphere (CLaMS), *Geosci. Model Dev.*, 7(6), 2895–2916, doi:10.5194/gmd-7-2895-2014.
- Randel, W. J., R. R. Garcia, N. Calvo, and D. Marsh (2009), ENSO influence on zonal mean temperature and ozone in the tropical lower stratosphere, *Geophys. Res. Lett.*, 36, L15822, doi:10.1029/2009GL039343.
- Riese, M., F. Ploeger, A. Rap, B. Vogel, P. Konopka, M. Dameris, and P. Forster (2012), Impact of uncertainties in atmospheric mixing on simulated UTLS composition and related radiative effects, *J. Geophys. Res.*, 117, D16305, doi:10.1029/2012JD017751.
- Scaife, A. A., N. Butchart, D. R. Jackson, and R. Swinbank (2003), Can changes in ENSO activity help to explain increasing stratospheric water vapor?, *Geophys. Res. Lett.*, 30(17), 1880, doi:10.1029/2003GL017591.
- Schieferdecker, T., S. Lossow, G. P. Stiller, and T. von Clarmann (2015), Is there a solar signal in lower stratospheric water vapour?, *Atmos. Chem. Phys.*, 15, 9851–9863, doi:10.5194/acp-15-9851-2015.
- Solomon, S., K. Rosenlof, R. Portmann, J. Daniel, S. Davis, T. Sanford, and G.-K. Plattner (2010), Contributions of stratospheric water vapor to decadal changes in the rate of global warming, *Science*, 327, 1219–1223, doi:10.1126/science.1182488.
- Tao, M., P. Konopka, F. Ploeger, M. Riese, R. Müller, and C. Volk (2015), Impact of stratospheric major warmings and the quasi-biennial oscillation on the variability of stratospheric water vapor, *Geophys. Res. Lett.*, 42, 4599–4607, doi:10.1002/2015GL064443.
- Waugh, D. W., and L. M. Polvani (2000), Climatology of intrusions into the tropical upper troposphere, *Geophys. Res. Lett.*, 27, 3857–3860.
- Wolter, K. (1987), The Southern Oscillation in surface circulation and climate over the tropical Atlantic, Eastern Pacific, and Indian Oceans as captured by Cluster analysis., *J. Clim. Appl. Meteorol.*, 26(6), 540–558.
- Yang, H., G. Chen, and D. I. V. Domeisen (2014), Sensitivities of the lower-stratospheric transport and mixing to tropical SST heating, *J. Atmos. Sci.*, 71, 2674–2694.
- Yeh, S., J. Kug, B. Dewitte, M. Kwon, B. Kirtman, and F. Jin (2009), El Niño in a changing climate, *Nature*, 461, 511–514, doi:10.1038/nature08316.